Dyes and Pigments 168 (2019) 257–263

Contents lists available at ScienceDirect

Dyes and Pigments

journal homepage: www.elsevier.com/locate/dyepig

Azadipyrromethene-based near-IR dyes with styryl substituents at the pyrrolic positions for organic photovoltaic applications

Roshan Fernando, Sandra Pejić, Anna Thomsen, Chunlai Wang, Geneviève Sauvé*

Department of Chemistry, Case Western Reserve University, Cleveland, OH, 44122, USA

ARTICLE INFO

Keywords:
Non fullerene acceptor
Organic solar cell
Homoleptic zinc complex
Aza-BODIPY
Charge carrier mobility

ABSTRACT

Azadipyrromethene dyes are attractive building blocks for the development of near-IR dyes, with applications ranging from biosensing, photodynamic therapy and solar energy conversion. In particular, Zn(II) *bis*(2,8-diphenylethynyl 1,3,7,9 tetraphenylazadipyrromethene) complexes are promising *n*-type non-fullerene electron acceptors for organic photovoltaics. Here, the triple bond in phenylethynyl pyrrolic substituents is replaced with a double bond. The UV–Vis absorption spectra were not significantly different, indicating that both the double and triple bond similarly extend the conjugation of ADP. Interestingly, the Zn(II) complex with styryl substituents ($Zn(WS6)_2$) showed emission in the near IR, with a λ_{max} of 773 nm. The BF_2^+ chelate also emitted in the near IR with a λ_{max} of 815 nm, but the emission was very weak. Cyclic voltammetry revealed that double bond compounds were easier to oxidize than un-substituted ADP analogues, and unlike with triple bond, were not easier to reduce. In organic photovoltaics, the $Zn(WS6)_2$ did not perform as well as the $Zn(WS3)_2$ analogue, showing unfavorable film morphology when blended with P3HT and low blend electron mobility of 2×10^{-8} $cm^2V^{-1}s^{-1}$ by SCLC, compared to 1×10^{-7} $cm^2V^{-1}s^{-1}$ in neat film. The hole mobility of $Zn(WS6)_2$ in neat films is 6×10^{-5} $cm^2V^{-1}s^{-1}$, higher than its electron mobility, suggesting its potential as p-type material as well. Further work in finding an appropriate n-type polymer acceptor is required to confirm this hypothesis. Using a triple bond at the pyrrolic positions is therefore better than a double bond for the development of *n*-type materials based on ADP dyes.

1. Introduction

Azadipyrromethenes (ADP) are bidentate ligands (−1 charge) that chelate Lewis acid main group or *d*-block transition metals. They have strong absorption in the visible to NIR range, despite their relatively small π-conjugated system, making them attractive for the development of red to NIR absorption dyes for photodynamic therapy, biosensing and solar energy conversion applications [1,2]. These dyes are often synthesized as the tetraphenylazadipyrromethene derivatives, Fig. 1, due to their easy synthesis and ability to symmetrically substitute the phenyl groups [3]. These dyes are usually coordinated with borondifluoride (BF_2^+) because of their advantageous photophysical properties such as strong NIR light absorption and high emission quantum yields [4]. We have explored ADP as building blocks for the development of *n*-type semiconductors for organic photovoltaic applications (OPVs), because they not only strongly absorb in the visible to near IR region of the solar spectra, but also have high electron affinity [5]. Their properties can be tuned by substitutions, ring fusion, and chelation [1,2].

To extend the π-conjugation of ADP dyes, conjugated groups can be incorporated at the *para* position of the phenyl groups, or at the pyrrolic positions, with a greater red-shift observed when using pyrrolic substitutions [6–10]. Aryl groups directly installed to the ADP pyrrolic positions do not extend conjugation because they twist out-of-plane due to steric hindrance with the proximal and distal phenyls. To avoid this problem, we incorporated a triple bond between the ADP core and the aryl group. This pyrrolic substitution successfully red-shifted the absorption spectra of both polymeric and molecular ADP-based dyes [7–9,11]. In particular, ADP dyes with pyrrolic phenylethynyl groups (bidentate ligand named WS3) resulted in absorption maximum in solution of 610, 732 and 674 nm for the free ligand (H(WS3)), BF_2^+ chelate (BF_2(WS3)) and Zn(II) chelate ($Zn(WS3)_2$), respectively [9]. When these dyes were tested as non-fullerene electron acceptor in organic photovoltaics (OPV, using poly(3-hexylthiophene) or P3HT as the electron donor), both the free ligand and BF_2^+ chelates gave near 0% efficiency due to poor blend morphology with P3HT. On the other hand, $Zn(WS3)_2$ worked well, with a maximum power conversion efficiency (PCE) of 4% [12]. The large improvement in performance is mainly due to a better blend morphology with P3HT: the non-planar 3D shape of the distorted tetrahedral Zn(II) ADP-based complex combined with the phenylethynyl groups prevented strong aggregation of the

* Corresponding author.
E-mail address: genevieve.sauve@case.edu (G. Sauvé).

https://doi.org/10.1016/j.dyepig.2019.04.067
Received 12 December 2018; Received in revised form 25 April 2019; Accepted 29 April 2019
Available online 02 May 2019
0143-7208/

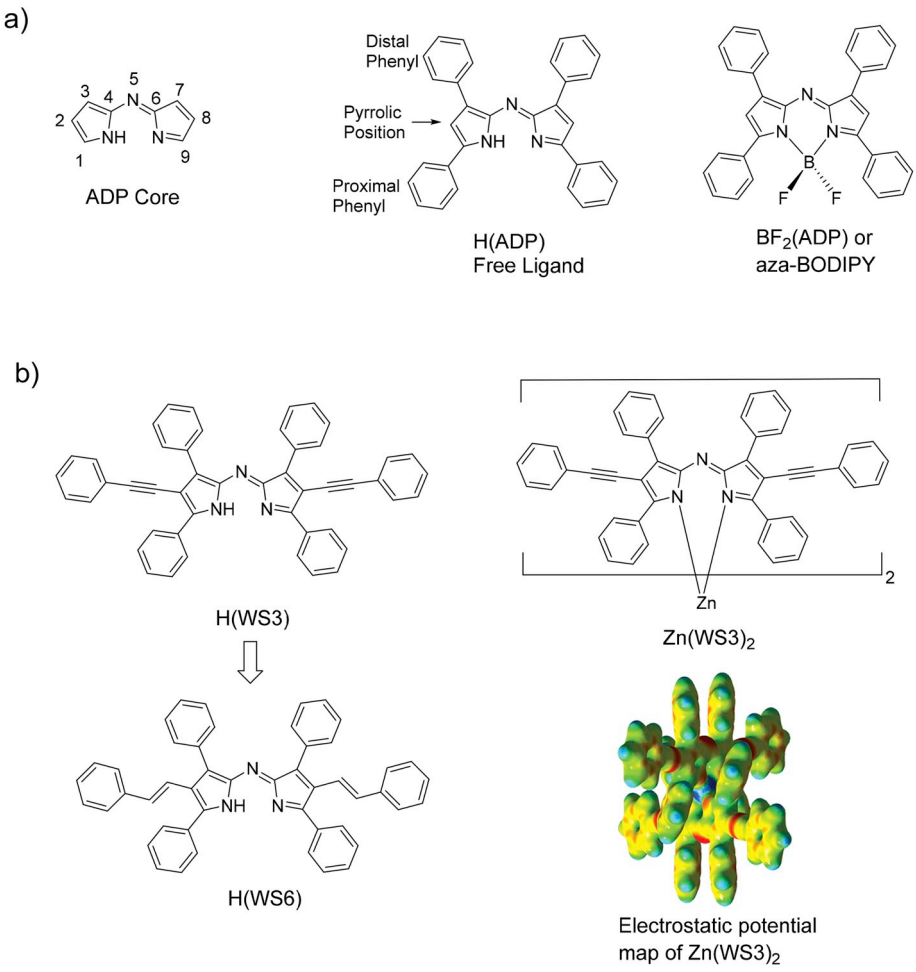

Fig. 1. a) ADP core, 1,3,7,9-tetraphenylazadipyrromethene free ligand and BF_2^+ chelate. b) Free ligand with pyrrolic phenylethynyl substitutions (H(WS3)), the zinc complex $Zn(WS3)_2$ and its optimized geometry (electrostatic potential map), and the free ligand where the triple bonds are replaced with double bonds (H(WS6)).

acceptor without impairing P3HT self-assembly. This results in a favorable blend morphology that resembles that of well-studied P3HT and [6,6]-phenyl-C61-butyric acid methyl ester (PCBM) blends. Incorporating either aryl or arylethynyl groups at the pyrrolic position resulted in similar blend morphology, with PCE in the 2–4% range, illustrating the generality of this substitution to tune self-aggregation and obtain a favorable blend morphology with P3HT [9,13].

One question that emerged is: what if we replaced the triple bond in phenylethynyl with a double bond? We do not expect photochemical isomerization reactions under ambient lighting conditions. Our previous DFT calculations predict slightly higher internal reorganization energy with the double bond than with the triple bond[14]. Our calculations also predict higher HOMO and LUMO energy levels and smaller HOMO-LUMO gap with the double bond than with the triple bond. Here, we synthesized an ADP ligand with styryl substituents at the pyrrolic positions and coordinated it with BF_2^+ and Zn(II). The optical, electrochemical, and photovoltaic properties of the new compounds are investigated and compared with the properties of the phenylethynyl-substituted analogues.

2. Experimental

2.1. Materials and methods

Solvents and reagents were purchased from commercial suppliers, Fischer or Aldrich, and used without further purification unless indicated. Azadipyrromethene (H(ADP)) and iodinated H(ADP) ($ADPI_2$) was synthesized according to published methods.[3,8] ^1H, ^{13}C and ^{19}F NMR spectra were recorded on a Varian AS-400 spectrometer. Chemical shifts (^1H) were reported in parts-per-million relative to $Si(CH_3)_4$. Elemental analysis (C, H, and N) was performed using optimum combustion conditions (Robertson Microlit Laboratories). UV/Vis spectra were collected on a Cary 500 spectrophotometer in HPLC grade chloroform or on 1 cm wide glass plate. Fluorescence spectra were collected on a Cary Eclipse fluorescence spectrophotometer. Films were spin-coated at 600 rpm for 60 s from 30 mg/mL chloroform solutions onto glass substrates. MALDI-TOF MS spectra were acquired in reflective negative mode on a Bruker Autoflex III Smartbeam MALDI-TOF TOF spectrometer. Cyclic voltammetry measurements were performed at room temperature using 0.1 M Bu_4NPF_6 in dry dichloromethane (distilled over CaH_2) as the electrolyte and ferrocene as the internal standard. The solutions were purged with dry nitrogen for 10 min prior to the measurement. Glassy carbon (GC) working electrodes were polished with 0.05 μm alumina, thoroughly cleaned and dried. Platinum wires were used as the counter and reference electrodes. All scans were performed at a scan rate of 0.1 V/s. The $E_{1/2}$ values versus ferrocene/ferrocenium (Fc/Fc^+) were calculated by setting the $E_{1/2}$ of Fc/Fc^+ to 0.0 V.

2.2. Synthesis of free ligand, H(WS6)

trans-phenylvinylboronic acid (127 mg, 0.855 mmol) and $ADPI_2$ (200 mg, 0.285 mmol) were charged into a dry 50 mL Schlenk flask and put under vacuum for 10 min. The flask was evacuated and refilled with N_2 three times. Dry chlorobenzene (20 mL) was added via a syringe.

The solvent was stirred and bubbled with N_2 for 5 min before adding the catalyst, $Pd(PPh_3)_4$ (57 mg, 10% mmol) inside a glove box. The reaction mixture was stirred for 15 min under N_2 at room temperature. Then a de-gassed aqueous solution (4 mL) of K_2CO_3 (280 mg) and Bu_4NBr (20 mg) was added to the reaction mixture via a syringe under N_2. The mixture was then heated at 80 °C for 24 h under N_2. After 24 h, portions of *trans*-phenylvinylboronic acid (65 mg) and $Pd(PPh_3)_4$ (33 mg) were added and heating was continued for another 24 h. The deep blue solution, which was initially purple, was cooled down to room temperature before pouring into methanol (500 mL) to precipitate. The precipitate was collected by vacuum filtration, dissolved in dichloromethane (300 mL) and passed through a Celite pad. The filtrate was then rotovaped to concentrate and poured into methanol (300 mL) to re-precipitate. The product was collected by vacuum filtration and washed with ether (300 mL) and further purified by Soxhlet extraction following the solvent sequence acetonitrile (15 h), hexanes (2 h) and dichloromethane (2 h). The dichloromethane fraction was rotovaped to obtain the pure product as a deep blue solid. Yield: 85 mg, 46%. ^{1}H NMR (400 MHz, CD_2Cl_2, δ): 7.80–7.82 (d, J = 8.0 Hz, 4H), 7.66–7.68 (d, J = 8.0 Hz, 4H), 7.48–7.54 (m, 6H), 7.38–7.42 (t, J = 8 Hz, 4H), 7.33–7.35 (d, J = 8 Hz, 4H), 7.27–7.29 (d, J = 8 Hz, 6H), 7.19–7.24 (m, 2H), 7.14–7.18 (d, J = 16 Hz, 2H), 6.57–6.61 (d, J = 16 Hz, 2H). ^{13}C NMR (500 MHz, CD_2Cl_2, δ): 149.97, 138.92, 138.13, 134.07, 133.88, 133.59, 131.51, 130.11, 129.36, 129.22, 129.15, 128.33, 128.11, 128.07, 126.73, 120.90, 100.57. MALDI-TOF MS: *m/z* calcd for $C_{48}H_{35}N_3$ 653.28, found 652.12. Elem. anal. calcd: C, 88.18; H, 5.40; N, 6.43; found: C, 87.92; H, 5.39; N, 6.38.

2.3. Synthesis of Zn(II) complex, Zn(WS6)$_2$

In a 100 mL three-necked flask connected with a reflux condenser, H(WS6) (100 mg, 0.152 mmol) was dissolved in anhydrous tetrahydrofuran (10 mL) under N_2. To this dark blue solution, anhydrous NaH (4.05 mg, 0.168 mmol) was added and the mixture was heated to 60 °C. The solution turned into a bright blue solution. After 24 h, anhydrous $ZnCl_2$ (11.5 mg, 0.084 mmol) was added and heating was continued for another 24 h. The mixture turned back into a dark blue color. The mixture was then cooled to room temperature and dissolved in dichloromethane (300 mL). This solution was passed through a Celite pad and the filtrate was collected. The crude product was obtained by rotary evaporation of dichloromethane. The crude product was purified by Silica flash chromatography using dichloromethane/hexane mixture as the eluent (started with 80% hexane and gradually decreased to 60%). After removal of solvents, the final pure product was obtained as a dark blue solid. Yield: 30 mg, 29%. ^{1}H NMR (500 MHz, CD_2Cl_2, δ) 7.53 (bs, 8H), 7.44 (bs, 8H), 7.38 (bs, 12H), 7.16–7.21 (bm, 32H), 6.94–6.97 (d, J = 12 Hz, 4H), 6.39–6.42 (d, J = 12 Hz, 4H). ^{13}C NMR (500 MHz, CD_2Cl_2, δ): 160.96, 147.50, 141.86, 138.45, 134.61, 134.43, 131.68, 131.45, 129.52, 129.39, 129.04, 128.41, 128.17, 127.77, 127.69, 127.67, 126.46, 121.21. MALDI-TOF MS: *m/z* calcd for $C_{96}H_{68}N_6Zn$ 1369.48, found 1368.84. Elem. anal. calcd: C, 84.10; H, 5.00; N, 6.13; found: C, 83.98; H, 5.27; N, 5.88.

2.4. Photovoltaic fabrication and characterization

Photovoltaic properties were studied using the inverted configuration: ITO/ZnO/P3HT:Acceptor/MoO_3/Ag. ITO-coated glass substrates (R = 15Ω/sq) were cleaned stepwise in soapy water, DI water, acetone and isopropanol under ultrasonication for 15 min followed by UV-ozone treatment at 80 °C for 15 min. A ZnO layer was prepared from a precursor solution of 0.25 M zinc acetate dihydrate in 0.25 M ethanolamine and 2-methoxyethanol by spin coating at 4000 rpm for 40 s, then heated at 150 °C for 7 min. The photoactive layers were spin coated inside the glovebox (PureLabHE) at 1000 rpm for 40 s followed by 2000 rpm for 2 s from a blend solution with a total concentration of 20 mg/mL in *o*-DCB. The solutions were filtered through a 0.45 μm PTFE filter prior to spin coating. All acceptors were blended with P3HT in 1:0.7 ratios. The photoactive layers were pre-annealed at 120 °C for 30 min followed by deposition of MoO_3 (10 nm) and Ag (80 nm) under a vacuum pressure of 3×10^{-5} Torr using the Angstrom Engineering Evovac Deposition System. Solar cell measurements were performed using an Oriel Sol2A solar simulator (AM 1.5, 100 mW/cm^2) and Keithley 2400 source meter inside the glovebox. The devices have a total effective area of 0.20 cm^2. Incident Photon-to-Charge Carrier Efficiency was measured in air on fully constructed devices using a QEX10 Quantum Efficiency Measurement System.

2.5. Space-charge limited current measurements

For single-carrier device fabrication, ITO-coated glass substrates (R = 15 Ω/sq) were cleaned as previously mentioned. For hole-only devices with an ITO/PEDOT:PSS/active layer/MoO_3/Ag structure, a layer of PEDOT:PSS was prepared by filtering through a 0.45 μm PTFE filter followed by spin coating at 4000 rpm for 60 s and heated at 150 °C for 10 min. The active layers were prepared in the same manner as for the photoactive layers. For electron-only devices with an ITO/ZnO/active layer/Ca/Al structure, the ZnO and active layer film formation was performed as previously described. Calcium (30 nm) and Al (100 nm) were thermally deposited. Dark current measurements for both architectures were performed using a Keithley 2400 source meter inside the glovebox. The devices have a total effective area of 0.20 cm^2.

2.6. Atomic force microscopy (AFM)

AFM was performed on the photoactive layer of photovoltaic devices using a Bruker Veeco Digital Instruments Dimension 3100 microscope and a Nanoscope Illa controller in tapping mode. WSxM 5.0 Develop 8.0 was used to analyze the AFM images [15].

3. Results and discussion

3.1. Synthesis

The synthesis of the styryl substituted free ligand and chelates is shown in Scheme 1. The free ligand H(WS6) was obtained by reacting the iodinated ADP ligand with *trans*-phenylvinylboronic acid under Suzuki coupling conditions. To increase yields, more *trans*-phenylvinylboronic acid and catalyst were added after 24 h and continued to react for an additional 24 h. The blue product H(WS6) was purified by Soxhlet extractions, recovered from the dichloromethane fraction and isolated in 46% yield. The BF_2^+ chelate BF_2(WS6) was synthesized using the literature procedure by reacting the free ligand with trifluoroboron etherate in 59% yield. The homoleptic zinc(II) complex Zn(WS6)$_2$ was synthesized using sodium hydride followed by zinc chloride. The sodium hydride deprotonates the amine of the ADP core leaving $Na^+(ADP^-)$ with the sodium acting as a good leaving group for the zinc(II). The method consistently gives higher yields for zinc chelating to azadipyrromethene than the more widely used method based on zinc acetate. The product was purified by column chromatography and isolated as a blue solid in 29% yield. NMR, MALDI-TOF MS and elemental analysis confirmed the compounds identity and purity. ^{1}H NMR of BF_2(WS6) and Zn(WS6)$_2$ show two doublets due to the protons on the double bond of the styryl substituents in the 6.4–7.0 ppm range, whereas they overlap with other signals in spectra for H(WS6). The ^{19}F NMR of BF_2(WS6) shows a quartet around 133 ppm, consistent with the tetracoordinated state of boron. The mass of Zn(WS6)$_2$ found by MALDI-TOF, 1369.47 *m/z*, is close to the calculated mass 1368.48.

3.2. Optical properties

Fig. 2 depicts the absorption spectra of the new ligand and its chelates in chloroform, and the optical properties are summarized in

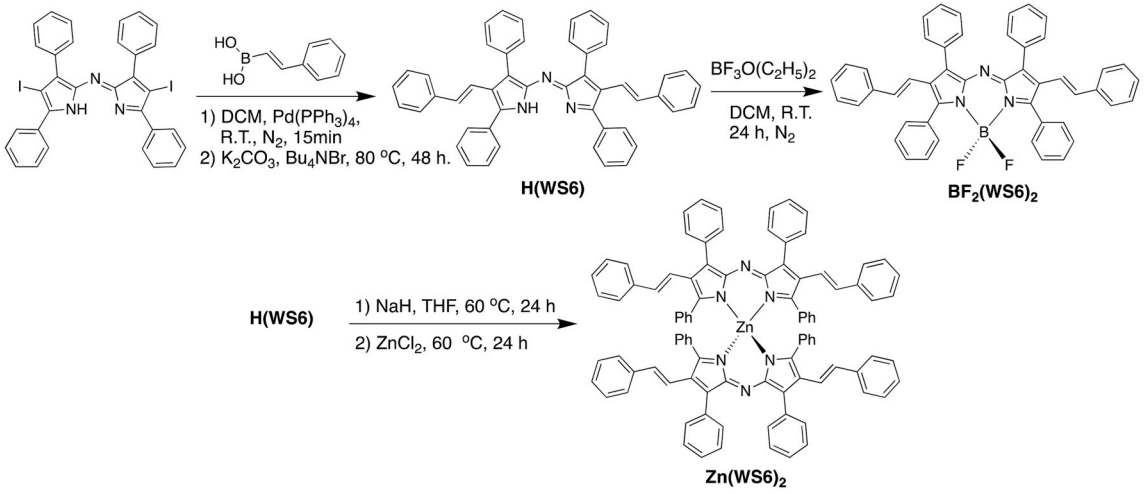

Scheme 1. Synthesis of styryl-substituted ADP and its chelates.

Table 1. The free ligand H(WS6) shows an absorption band at 305 nm and at 603 nm with absorptivity coefficients of 39 $kM^{-1}cm^{-1}$and 43 $kM^{-1}cm^{-1}$, respectively. Chelation with BF_2^+ red-shifts the visible absorption band by 133 nm, to a λ_{max} of 736 nm with a maximum absorptivity coefficient of 39 $kM^{-1}cm^{-1}$. The homoleptic zinc complex shows strong absorptions at 302 nm and 688 nm, with high absorptivity coefficients of 74 $kM^{-1}cm^{-1}$ and 91 $kM^{-1}cm^{-1}$, respectively. As with other related azadipyrromethene complexes, BF_2^+ chelation gave the most red-shifted absorption, with a maximum in near-IR whereas the homoleptic zinc(II) complex gave the strongest absorptivity coefficient.

Table 1 also includes the optical data for the phenylethynyl-substituted free ligand, BF_2^+ and Zn(II) chelates for comparison. The absorption and absorption coefficients tend to be similar whether the compound is substituted with styryl or phenylethynyl, indicating that both have similar conjugation length. Fig. 3 compares the absorption spectra of $Zn(ADP)_2$, $Zn(WS3)_2$ and $Zn(WS6)_2$ in solution and film. The absorption spectra were normalized for direct comparison. Both $Zn(WS3)_2$ and $Zn(WS6)_2$ spectra are similar in solution and film, and are both red-shifted compared to $Zn(ADP)_2$, further demonstrating that both pyrrolic substituents extend the conjugation length similarly. Comparing the spectra of solution and film, we note a large red-shift upon film formation for $Zn(ADP)_2$, consistent with its ability to aggregate, whereas the pyrrolic-substituted complexes exhibit a smaller red-shift upon film formation than $Zn(ADP)_2$, consistent with our previous results with pyrrolic-substituted complexes of ADP [9].

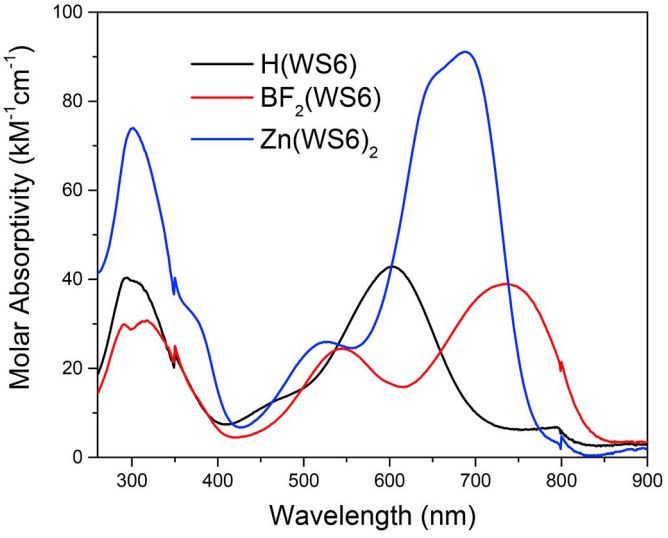

Fig. 2. Absorption spectra of new compounds in solution.

Fig. 4 depicts the emission spectra of the new compounds. The free ligand emitted weakly around 724 nm and the BF_2^+ chelate emitted weakly at 815 nm, with a quantum yield (QY) too low to measure accurately. In contrast, the QY for the unsubstituted BF_2(ADP) is 0.34. The styryl groups therefore provide a deactivation pathway for fluorescence, though not as pronounced as the phenylethynyl groups. To our surprise, the styryl-substituted $Zn(WS6)_2$ showed emission at 773 nm in solution with a QY of 0.003 (using BF_2(ADP) as standard), and weak emission in film at 793 nm. The small Stokes shift suggests that the Zn complex is very rigid, consistent with the very low internal reorganization energies calculated for this complex [14]. To our knowledge, $Zn(WS6)_2$ is the only ADP-based zinc complex that shows emission, and the only one where the emission of the Zn complex is stronger than that of the BF_2^+ chelate.

3.3. Electrochemistry

The electrochemical properties of the new compounds were investigated by cyclic voltammetry (CV) in dichloromethane, using ferrocene/ferrocenium as the internal reference. The cyclic voltammograms are shown in Fig. 5. The free ligand has two irreversible reductions and one irreversible oxidation events. The BF_2^+ chelate has two reversible reductions and one irreversible oxidation events and the Zn chelate has two closely spaced reductions and two quasi-reversible oxidation events. Oxidations and reductions tend to be less reversible than for the phenylethynyl substituted related compounds. The electrochemical properties are summarized in Table 2. Table 2 also includes the data for the phenylethynyl-substituted compounds for comparison.

Fig. 6 compares the estimated HOMO and LUMO energy levels for the Zn complexes in solution using the $E_{1/2}$ values and −5.1 eV for Fc/Fc^+. Compared to un-substituted $Zn(ADP)_2$, the $Zn(WS6)_2$ has a slightly higher HOMO and a similar LUMO energy levels. This is in contrast with the phenylethynyl substituent, which stabilizes both the HOMO and LUMO levels. Phenylethynyl groups are therefore better suited than styryl groups for the design of electron acceptors.

3.4. Organic photovoltaics

Since the homoleptic zinc(II) complexes worked well as an electron acceptor (or *n*-type) in organic photovoltaic (OPV) when blended with P3HT, we tested $Zn(WS6)_2$ in OPVs using regioregular poly(3-hexylthiophene) (P3HT) as the electron donor (or *p*-type). Devices were

Table 1
Optical properties of free ligand and chelates with phenylethynyl and styryl substituents.

Compound	Solution			Film	
	Absorption λ_{max}, nm (ε, $kM^{-1}cm^{-1}$)	Absorption λ_{onset}, nm ($E_{g,opt}$, eV)	Emission λ_{max}, nm	λ_{max} nm	λ_{onset}, nm ($E_{g,opt}$, eV)
H(WS3)*	309 (39), 610 (42)	676 (1.83)	N/A	585	775 (1.60)
H(WS6)	305 (39), 603 (43)	703 (1.76)	724	498	709 (1.75)
BF_2(WS3)*	306 (25), 732 (49)	782 (1.59)	792	763	845 (1.47)
BF_2(WS6)	312 (31), 543 (24), 736 (39)	830 (1.49)	815	718	852 (1.46)
$Zn(WS3)_2$*	309 (39), 644 (99), 674 (105)	757 (1.64)	N/A	696	785 (1.58)
$Zn(WS6)_2$	302 (74), 655 (86), 688 (91)	762 (1.63)	773	705	787 (1.57)

* Literature values [9].
N/A = not detectable.

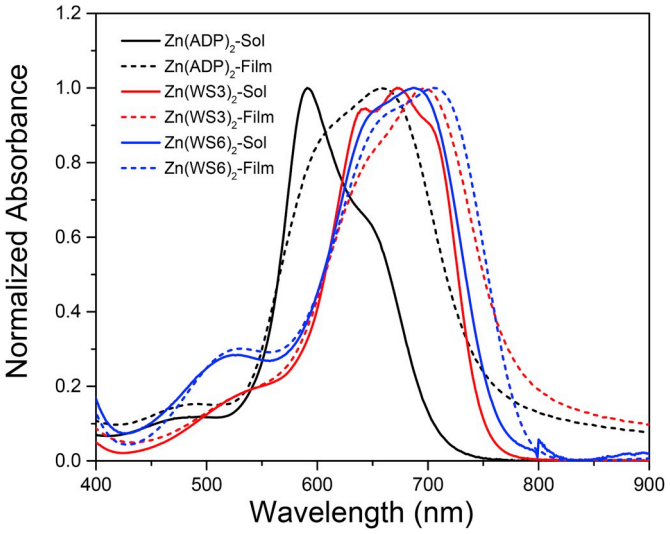

Fig. 3. Comparison of absorption spectra for the homoleptic zinc complexes in solution and film.

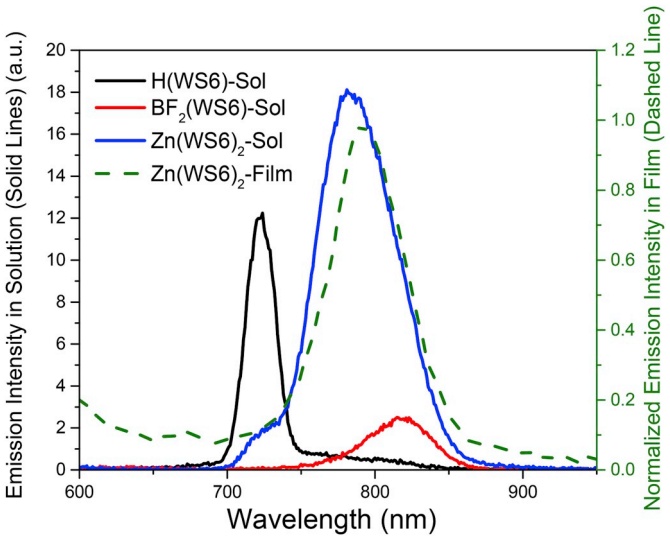

Fig. 4. Emission spectra for WS6 compounds in solutions and for $Zn(WS6)_2$ in film. Solution concentration for all compounds was 2 μM and film thickness for $Zn(WS6)_2$ was 70 nm.

fabricated using the inverted geometry and processing conditions that worked well for $Zn(WS3)_2$. Fig. 7 shows the current-voltage curves for the best devices obtained and Table 3 summarizes the performance parameters. While $Zn(WS6)_2$ slightly outperformed $Zn(ADP)_2$, it showed a lower short circuit current (J_{SC}), fill factor (FF) and power

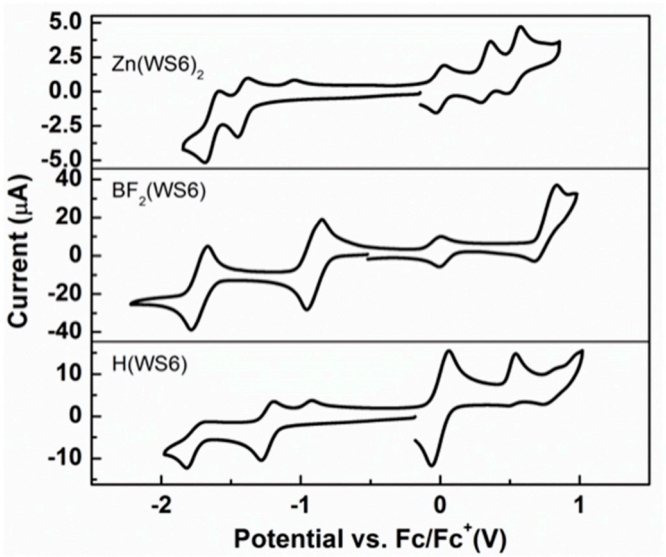

Fig. 5. Cyclic voltammograms for new compounds in dichloromethane using ferrocene/ferrocenium as internal standard.

conversion efficiency (PCE) than $Zn(WS3)_2$, with a PCE of 1.4%. AFM images of the OPV active layer surface, Fig. 8, show that while the P3HT:$Zn(WS3)_2$ blend had typical P3HT nanofibril formation for efficient hole transport, the P3HT:$Zn(WS6)_2$ had a less favorable nodular-like morphology. Interestingly, the P3HT:$Zn(WS6)_2$ film was very smooth, with a surface roughness of 0.68 nm from the 1 × 1 μm images. In contrast, $Zn(WS3)_2$:P3HT films had a surface roughness of 12 nm, which is more similar to the roughness of P3HT:PCBM [16]. We hypothesize that the $Zn(WS6)_2$ is too miscible with P3HT, thus preventing P3HT from π-stacking and form nanofibrils.

Charge carrier mobility was estimated by Space Charge Limited-Current method in hole and electron only devices. Hole mobility measurement used a device structure of ITO/PEDTO:PSS/Active layer/MoO_3/Ag and electron mobility measurement used a device structure of ITO/ZnO/Active layer/Ca/Al. The SCLC were investigated from current density-voltage characteristics (J -V curve) in the dark. Mobilities were calculated with Mott-Gurney law under the trap free SCLCs situation $J = 9\varepsilon_r\varepsilon_0\mu V^2/(8L^3)$ [17], where J is the current density, ε_0 is the permittivity of free space, ε_r is the relative permittivity of the material, μ is the charge carrier mobility, V is the effective voltage, and L is the thickness of the active layer. The SCLC graphs are shown in Figs. S9–12 and results are listed in Table 4. In neat films, $Zn(WS6)_2$ had a hole and electron mobility of 5.7×10^{-5} $cm^2V^{-1}s^{-1}$ and 1.4×10^{-7} $cm^2V^{-1}s^{-1}$, respectively. While the hole mobility is approaching 10^{-4} $cm^2V^{-1}s^{-1}$, the electron mobility is low. This suggests that $Zn(WS6)_2$ may be more suited as a *p*-type material. In blend films, the hole mobility was 9.0×10^{-5} $cm^2V^{-1}s^{-1}$, a bit low for P3HT-based devices,

Table 2
Electrochemical properties of chelates with phenylethynyl and styryl substituents.

Compound	$E_{1/2}$ reduction, V vs Fc/Fc^+	E(p,c), V vs. Fc/Fc^+	$E_{1/2}$ oxidation, V vs Fc/Fc^+	E(p,a), V vs Fc/Fc^+	$E_{g,elect}$, eV[a]
H(WS6)	−1.23, −1.75	−1.27, −1.82	0.52	0.54	1.75
BF_2(WS3)	−0.79, −1.59	−0.95, −1.75	N/A	1.08	N/A
BF_2(WS6)	−0.90, −1.73	−0.95, −1.79	0.78	0.84	1.68
$Zn(WS3)_2$[b]	−1.25, −1.47	−1.33, −1.55	0.50, 0.77	0.58, 0.86	1.75
$Zn(WS6)_2$	−1.42, −1.64	−1.45, −1.68	0.33, 0.52	0.37, 0.59	1.75

N/A: not available from CV curves.
[a] Obtained from $E_{1/2}$ values.
[b] Data borrowed from Mao et al. [12].

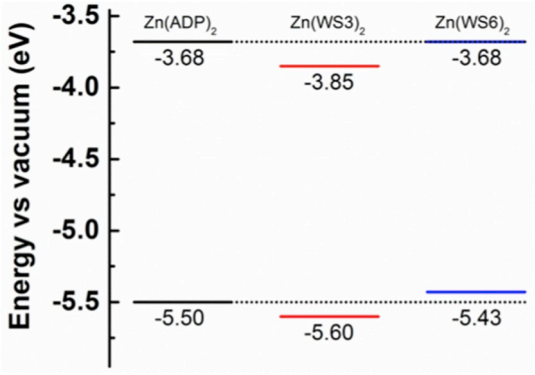

Fig. 6. Estimated HOMO and LUMO energy levels for the Zn complexes, using $E_{1/2}$ values for first oxidation and first reduction and −5.1 eV for Fc/Fc+.

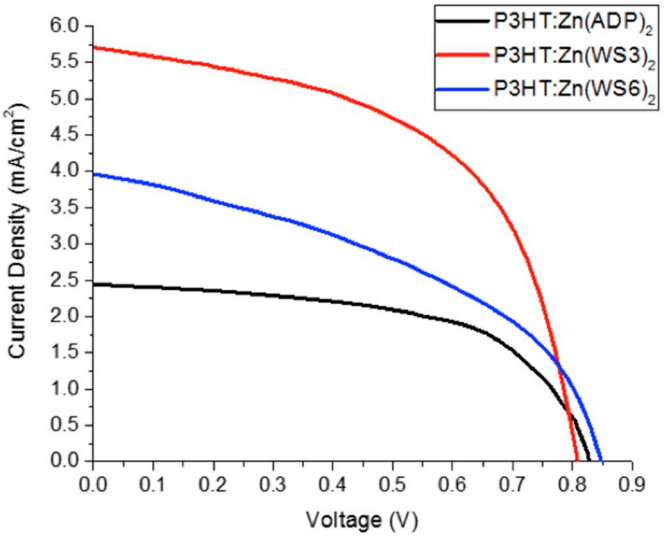

Fig. 7. Current density-voltage curves of best devices.

consistent with the unfavorable morphology seen by AFM. The electron mobility was about one order of magnitude lower in blends than in neat films, at 1.8×10^{-8} $cm^2V^{-1}s^{-1}$, also indicative of unfavorable blend morphology and consistent with the complex intermixed with P3HT. These results, combined with the estimated energy levels, suggest that the double bond is a poor choice for developing *n*-type materials based on these types of complexes.

Since our results suggest that $Zn(WS6)_2$ be considered as electron donor in OPVs, we have attempted to make devices by blending $Zn(WS6)_2$ with PCBM, but the resulting films were very uneven, probably because both materials are similarly shaped small molecules. As a result, we obtained poor devices with no photovoltaic effects. We then turned to a polymer acceptor, P(NDI2OD-P2), that we graciously obtained from Polyera. However, initial attempts also gave poor results. We hypothesized that these results are mainly due to morphological issues in the blend film. We note that azadipyrromethene-based dyes have been used as donor in vacuum-deposited organic solar cells using fullerene as the acceptor [18–20], so there is no fundamental reason to expect that $Zn(WS6)_2$ cannot also be used as donor given that the appropriate donor and processing conditions are found. Further investigations is thus required to fully evaluate the potential of this complex as donor in OPVs; such extensive work is beyond the scope of this paper.

4. Conclusions

We explored replacing the triple bond in phenylethynyl pyrrolic substituents with a double bond: styryl substituent. The UV–Vis absorption spectra were not significantly different, indicating that both the double and triple bond similarly extend the conjugation of ADP. The Zn(II) complex showed emission in the near IR, with a λ_{max} of 773 nm and a quantum yield of 0.003. To our knowledge, this is the first homoleptic Zn(II) complex of ADP that shows emission. The BF_2^+ chelate also emitted in the near IR with a λ_{max} of 815 nm, but the emission intensity was too low to accurately measure a quantum yield. Cyclic voltammetry revealed that double bond compounds were easier to oxidize than unsubstituted ADP analogues, and unlike with triple bond, were not easier to reduce. The redox events also tended to be less reversible in the double-bond containing systems than in the triple-bond containing systems, at least at the scan rate of 0.1 V/s. In organic photovoltaics, the $Zn(WS6)_2$ did not perform as well as the $Zn(WS3)_2$ analogue, showing unfavorable film morphology when blended with P3HT and low electron mobility. SCLC measurements of neat films of $Zn(WS6)_2$ shows a hole and electron mobility of 5.7×10^{-5} $cm^2V^{-1}s^{-1}$ and 1.4×10^{-7} $cm^2V^{-1}s^{-1}$, respectively, showing ambipolar behavior. The higher hole mobility suggests that $Zn(WS6)_2$ may be better suited as a *p*-type material. We conclude that using a triple bond is better than the double bond for the development of *n*-type materials based on ADP dyes.

Table 3
Performance parameters for P3HT:Zn(II) complexes organic solar cells. Best result and average for 6–10 devices.

Zn(II) complex	V_{OC} (V)	J_{SC} (mA cm^{-2})	FF	PCE (%)
$Zn(ADP)_2$	0.83 (0.83)	2.4 (2.4)	0.58 (0.55 ± 0.03)	1.2 (1.1 ± 0.1)
$Zn(WS3)_2$	0.81 (0.77 ± 0.04)	5.7 (5.4 ± 0.3)	0.55 (0.52 ± 0.02)	2.5 (2.1 ± 0.4)
$Zn(WS6)_2$	0.85 (0.83 ± 0.02)	4.0 (3.2 ± 0.7)	0.43 (0.42 ± 0.01)	1.4 (1.1 ± 0.3)

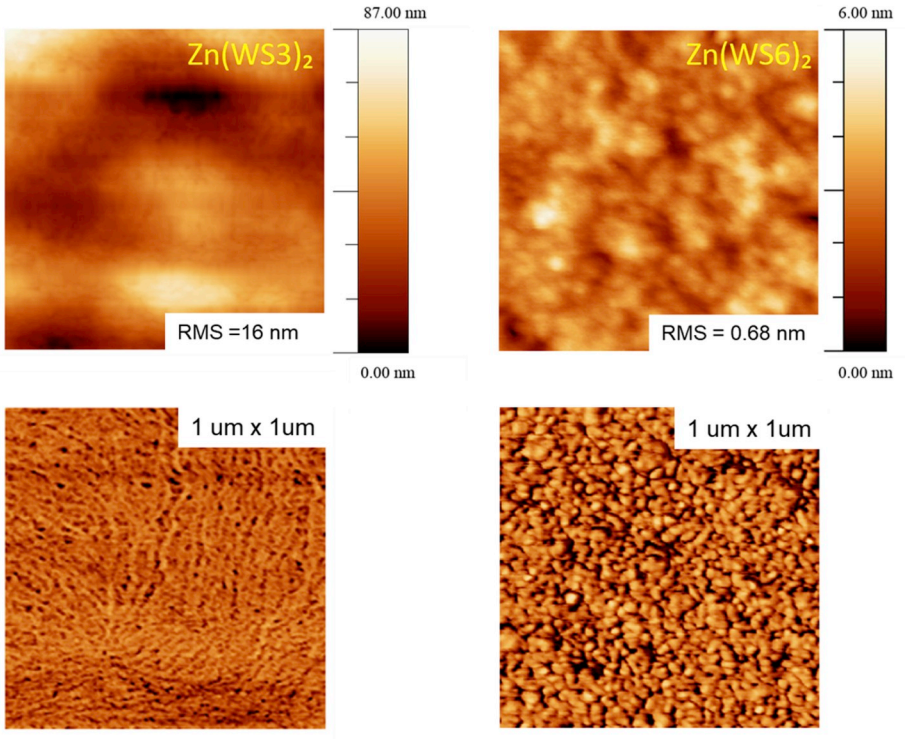

Fig. 8. 1 × 1 μm AFM images. Top: P3HT:$Zn(WS3)_2$ and P3HT:$Zn(WS6)_2$ height images. Bottom: P3HT:$Zn(WS3)_2$ and P3HT:$Zn(WS6)_2$ phase images.

Table 4
Charge carrier mobility for $Zn(WS6)_2$ complexes by SCLC method. The reported values are averages for 6–10 devices.

Material	Neat μ^+ ($cm^2\ V^{-1}\ s^{-1}$)	Neat μ^e ($cm^2\ V^{-1}\ s^{-1}$)	Blend μ^+ ($cm^2\ V^{-1}\ s^{-1}$)	Blend μ^e ($cm^2\ V^{-1}\ s^{-1}$)
$Zn(WS6)_2$	$(5.7 \pm 0.3) \times 10^{-5}$	$(1.4 \pm 0.1) \times 10^{-7}$	$(9.0 \pm 0.2) \times 10^{-5}$	$(1.8 \pm 0.1) \times 10^{-8}$

Acknowledgments

We are grateful to the National Science Foundation (CHEM 1148652) for funding this project, and the Case High Performance Computing Cluster for computing time, NSF MRI-0821515 for the MALDI-TOF/TOF and NSF MRI-1334048 for NMR instrumentation. The authors thank the Materials for Optoelectronics Research and Education (MORE) Center at CWRU for providing equipment for device work and Dr. Ina Martin for providing support for the fabrication and characterization of solar cells.

Appendix A. Supplementary data

Supplementary data to this article can be found online at https://doi.org/10.1016/j.dyepig.2019.04.067.

References

[1] Loudet A, Burgess K. Bodipy dyes and their derivatives: syntheses and spectroscopic properties. Chem Rev 2007;107:4891–932.
[2] Ge Y, O'Shea DF. Azadipyrromethenes: from traditional dye chemistry to leading edge applications. Chem Soc Rev 2016;45:3846–64.
[3] Gorman A, Killoran J, O'Shea C, Kenna T, Gallagher WM, O'Shea DF. In vitro demonstration of the heavy-atom effect for photodynamic therapy. J Am Chem Soc 2004;126:10619–31.
[4] Killoran J, Allen L, Gallagher JF, Gallagher WM, O'Shea DF. Synthesis of BF2 chelates of tetraarylazadipyrromethenes and evidence for their photodynamic therapeutic behaviour. Chem Commun 2002:1862–3.
[5] Partyka D, Deligonul N, Washington M, Gray T. Fac-tricarbonyl rhenium(I) azadipyrromethene complexes. Organometallics 2009;28:5837–40.
[6] Yoshii R, Nagai A, Chujo Y. Highly near-infrared photoluminescence from aza-borondipyrromethene-based conjugated polymers. J Polym Sci A Polym Chem 2010;48:5348–56.
[7] Gao L, Tang S, Zhu L, Sauve G. Synthesis and characterization of azadipyrromethene- alt- p-phenylene ethynylene conjugated polymers and their chelates. Macromolecules 2012;45:7404–12.
[8] Gao L, Senevirathna W, Sauve G. Azadipyrromethene-based conjugated oligomers with near-IR absorption and high electron affinity. Org Lett 2011;13:5354–7.
[9] Senevirathna W, Liao J-y, Mao Z, Gu J, Porter M, Wang C, Fernando R, Sauvé G. Synthesis, characterization and photovoltaic properties of azadipyrromethene-based acceptors: effect of pyrrolic substituents. J Mater Chem A 2015;3:4203–14.
[10] Daddario CM, Han Q, Zeller M, Sauvé G. Azadipyrromethene-based near-infrared dyes: effect of thienylethynyl substitution at the distal and proximal phenyl groups. Eur J Inorg Chem 2015;2015:3649–57.
[11] Senevirathna W, Sauve G. Introducing 3D conjugated acceptors with intense red absorption: homoleptic metal(II) complexes of di(phenylacetylene) azadipyrromethene. J Mater Chem C 2013;1:6684–94.
[12] Mao Z, Senevirathna W, Liao JY, Gu J, Kesava SV, Guo C, Gomez ED, Sauvé G. Azadipyrromethene-based Zn(II) complexes as nonplanar conjugated electron acceptors for organic photovoltaics. Adv Mater 2014;26:6290–4.
[13] Sauvé G, Fernando R. Beyond fullerenes: designing alternative molecular electron acceptors for solution-processable bulk heterojunction organic photovoltaics. J Phys Chem Lett 2015;6:3770–80.
[14] Senevirathna W, Daddario CM, Sauvé G. Density functional theory study predicts low reorganization energies for azadipyrromethene-based metal complexes. J Phys Chem Lett 2014;5:935–41.
[15] Horcas I, Fernandez R, Gomez-Rodriguez JM, Colchero J, Gomez-Herrero J, Baro AM. WSXM: a software for scanning probe microscopy and a tool for nanotechnology. Rev Sci Instrum 2007;78:013705.
[16] Li G, Shrotriya V, Huang J, Yao Y, Moriarty T, Emery K, Yang Y. High-efficiency solution processable polymer photovoltaic cells by self-organization of polymer blends. Nat Mater 2005;4:864–8.
[17] Unlu NA, Hacioglu SO, Hizalan G, Yildiz DE, Toppare L, Cirpan A. Benzodithiophene and benzotriazole bearing conjugated polymers for electrochromic and organic solar cell applications. J Electrochem Soc 2017;164:G71–6.
[18] Mueller T, Gresser R, Leo K, Riede M. Organic solar cells based on a novel infrared absorbing aza-bodipy dye. Sol Energy Mater Sol Cells 2012;99:176–81.
[19] Lorenz-Rothe M, Schellhammer KS, Jaegeler-Hoheisel T, Meerheim R, Kraner S, Hein MP, Schuenemann C, Tietze ML, Hummert M, Ortmann F, Cuniberti G, Koerner C, Leo K. From fluorine to fluorene-a route to thermally stable Aza-bodipys for organic solar cell application. Adv Electron Mater 2016;2:1600152.
[20] Leblebici SY, Catane L, Barclay DE, Olson T, Chen TL, Ma B. Near-infrared azadipyrromethenes as electron donor for efficient planar heterojunction organic solar cells. ACS Appl Mater Interfaces 2011;3:4469–74.